Journal of Alloys and Compounds 524 (2012) 5–12

Contents lists available at SciVerse ScienceDirect

Journal of Alloys and Compounds

journal homepage: www.elsevier.com/locate/jallcom

Reduced graphene oxide/CdS for efficiently photocatalystic degradation of methylene blue

Xinwei Wang[a,b], Hongwei Tian[a], Yan Yang[a], Huan Wang[a], Shumin Wang[a], Weitao Zheng[a,*], Yichun Liu[c]

[a] Department of Materials Science, Key Laboratory of Mobile Materials, MOE, State Key Laboratory of Superhard Materials, Jilin University, Changchun 130012, China
[b] School of Materials Science and Engineering, Changchun University of Science and Technology, Changchun 130022, China
[c] Center for Advanced Optoelectronic Functional Materials Research, Key Laboratory for UV-Emitting Materials and Technology of MOE, Northeast Normal University, 5268 Renmin Street, Changchun 130024, China

ARTICLE INFO

Article history:
Received 19 November 2011
Received in revised form 6 February 2012
Accepted 6 February 2012
Available online 16 February 2012

Keywords:
Reduced graphene oxide
Cadmium sulfide
Hybrid material
Photocatalytic activity

ABSTRACT

Reduced graphene oxide/cadmium sulfide (RGO/CdS) hybrid material was synthesized by a one-step solvothermal method, wherein graphene oxide (GO) was a supporting material on which CdS nanoparticles were distributed homogeneously, and cadmium acetate ($Cd(Ac)_2{\cdot}2H_2O$) was used as the CdS precursor. The supporting material RGO for CdS nanoparticles effectively enhanced their photocatalytic activities for the photodegradation of methylene blue in the aqueous solution. The optimum weight ratio of the GO to CdS in the hybrid material was 5.0%, which exhibited an excellent photodegradation efficiency (94%) and a better removal efficiency of total organic carbon (TOC) (57%), about 2.5 times and 5.1 times higher than that of pure CdS nanoparticles, respectively, under visible light (VL) irradiation. This improved photodegradation efficiency could be attributed to the increased adsorbability for methylene blue molecules, light absorption levels located in visible region, high charge transfer and separation ability, due to the introduction of a two-dimensional RGO network.

1. Introduction

Water pollutants, the most serious environmental contaminations, caused by synthetic textile dyes and other industrial dyestuffs, have led to an attracted extensive attention for wastewater treatment in the world. The dyes in water are commonly toxic and some of them are carcinogenic and mutagenic, resulting in adverse impact on human and animal health [1]. Photocatalysis as a more powerful method has attractive potential applications in the degradation of toxic water pollutants as well as the production of H_2 by water splitting [2–4]. However, so far, most photocatalytic degradation studies have focused on the use of nanosized oxide semiconductors photocatalysts [5–8]. These nanosized oxide semiconductors with wide band gaps (for example, for TiO_2, band gap (E_g) > 3.2 eV for anatase and 3.0 eV for rutile) mainly absorb ultraviolet (UV), which only accounts for about 4% of the solar radiation energy, while the visible light (VL) contributes to about 43% [9–12]. Therefore, the development of an effective photocatalyst with a high VL response for wastewater treatment remains a challenge.

Cadmium sulfide (CdS), as a VL-driven photocatalyst, has been extensively studied because of its relatively narrower bandgap (2.42 eV) than TiO_2 (3.2 eV) to facilitate the utilization of the VL. This makes CdS as a competitive candidate of photocatalysts having an excellent photodegradation property of organic or inorganic pollutants in water and air [13–17]. However, CdS particles are not stable and prone to aggregate, which results in a reduced surface area and a higher recombination rate of photoinduced electron–hole pairs to obstruct its large-scale application. To solve these problems, various investigations have been carried out to improve the efficiency of the photocatalytic activity for CdS.

Graphene, a novel two-dimensional (2D) carbonaceous material with honeycomb crystal structure and atom-thick layer features, has become a sparkling rising star on the horizon of materials science, due to its many potential applications in physical, chemical, biological, photoelectric, and catalytic fields [18–20]. The graphene has been employed as a support for many catalysts such as TiO_2 [21], $Ni(OH)_2$ [22], RuO_2 [23], and Fe_3O_4 [24]. Additionally, since chemical modified graphene with the excellent electronic conductivity and the high adsorption capacity, many researchers have used it as electron acceptor and supporting matrix for photocatalyst particles to improve the efficiency of the degradation of organic pollutants [25–29]. Recently, a few methods for decorating graphene with CdS nanoparticles have been reported. For example, Feng

* Corresponding author. Tel.: +86 431 85168246; fax: +86 431 85168246.
E-mail address: wtzheng@jlu.edu.cn (W. Zheng).

0925-8388/$ – see front matter © 2012 Elsevier B.V. All rights reserved.
doi:10.1016/j.jallcom.2012.02.058

et al. [30] have reported the synthesis of graphene nanosheets (GNs)/CdS nanocomposites via the π–π stacking interaction using benzyl mercaptan as the inter-linker. Pham et al. [31] have synthesized hybrid material containing graphene oxide (GO) and CdS quantum dots (CdS QDs) using an amidation reaction between the amino groups located on the CdS QDs surface and the acyl chloride groups bound to GO surface. Although these investigations provide a few feasible methods to obtain the hybrid materials, there is a problem about that the semiconductor nanoparticles and GNs always need to be bridged with short chain organic molecule linkers, which means that the synthesis process is complicated, and also an undesired electron barrier between semiconductor nanoparticles and GNs (or GO) may appear. Nevertheless, Cao et al. [32] have developed an one-step solvothermal method for synthesizing graphene/CdS QDs hybrid material with homogeneously distributed CdS QDs and excellent optoelectronic properties, using dimethyl sulfoxide (DMSO) as the sulfide source and the reducing agent. The solvothermal method can be used not only to synthesize GNs/CdS hybrid materials simply, but also to restrain the aggregation of either GNs or CdS nanoparticles effectively. Furthermore, this method can control the reduction degree of GO. As the reduced GO has a high charge transfer and separation rate, if CdS nanoparticles can be distributed homogeneously on the RGO, forming a hybrid RGO/CdS material, it can be expected that the photocatalytic activities for CdS nanoparticles will be strengthened. Nevertheless, the RGO containing a low content of oxygen-hydrophilic groups allows the hybrid material to be dispersed easily in water to a certain extent, which is required for the photocatalytic reaction [33]. To the best of our knowledge, so far, there are few investigations about the effect of the RGO on the degradation of organic pollution for CdS under VL irradiation, although there exist some reports on that a few carbon nanotube/CdS hybrid materials as photocatalysts have been used for photodegradation of organic pollution [1,34] as well as the photocatalytic H_2 production [35–39].

Herein, we employ a solvothermal technique to synthesize RGO/CdS hybrid material through direct growth of CdS on the RGO surface, and the degradation of methylene blue (MB) solution under VL irradiation for the obtained RGO/CdS is explored. Furthermore, the effect of the RGO content on the photocatalytic activity for CdS, and the electron-transfer mechanism for the photocatalytic RGO/CdS hybrid material are also discussed.

2. Experimental

2.1. Materials

Natural graphite powder (99 wt.% purity, Qingdao Yingshida Graphite Co. Ltd.) was used to prepare graphene oxide (GO), while $Cd(CH_3COO)_2{\cdot}2(H_2O)$ (99.99 wt.%, A. R., Shanghai Guoyao Chemicals Co., Ltd.) and dimethylsulfoxide (DMSO) (99.99 wt.%, A. R., Tianjin Henxing Chemicals Co., Ltd.) were the precursors to obtain CdS. $C_{16}H_{18}N_3S{\cdot}Cl$ (MB) (99.99 wt.%, A. R., Korea Duksan Pure Chemical Co., Ltd.) was employed as model pollutant. All other solvents were purchased from Beijing Beihua Chemicals Co., Ltd.

2.2. Synthesis of graphene oxide

Graphite oxide was synthesized from natural graphite powder by using a modified Hummers' method [40], and then, the exfoliation of graphite oxide to graphene oxide (GO) was achieved ultrasonically for 30 min (60 W). Finally, a homogeneous GO aqueous dispersion (0.5 mg/mL) was obtained and ready for further characterization. The detailed synthesis procedure of the GO had been described in ref [41].

2.3. Synthesis of CdS and RGO/CdS hybrid material

To synthesize RGO/CdS, a various amount of GO and 426 mg $Cd(Ac)_2{\cdot}2H_2O$ were dispersed in DMSO (150 mL) solution by vigorously stirring to form a stable suspension at ambient temperature. The weight ratios of GO to $Cd(Ac)_2{\cdot}2H_2O$ were fixed at 1.0%, 3.0%, 5.0%, 8.0% and 12.0%, and the obtained samples (RGO/CdS hybrid material) were named as RGOC*x* (*x* = 1.0, 3.0, 5.0, 8.0, 12.0). The obtained suspension was transferred into a polytetrafluoroethylene (PTFE)-lined stainless-steel autoclave (200 mL), and heated at 180 °C for 12 h. The dark-green precipitate was obtained through centrifugation at 5000 r/min, washed with ethanol and then acetone several times to remove the undecorated CdS nanoparticles. Finally, the products were dried under vacuum drier at 50 °C overnight before characterization. The formation process of RGO/CdS could be described as follows: during the temperature-rise period (<180 °C, <12 h), Cd–DMSO complex through Cd–S coordination was formed due to DMSO solution with a high polarization. After vigorous collision, the Cd–DMSO complex then bonded to oxy-functional groups (carboxyl or hydroxyl) on the GO under the condition of high temperature and pressure. Up to an elevated temperature (180 °C), S^{2-} anion reacted with Cd^{2+} to form CdS nanoparticles, due to the S═O and S—C bonds ruptured in the DMSO molecule to generate the S^{2-} anion slowly [42]. Therefore, these CdS nanoparticles will be immobilized on the RGO surface, as shown in Fig. 1. For comparison, pure CdS and RGO were also obtained via a similar process under the same experimental conditions.

2.4. Characterization

X-ray diffraction (XRD) experiments for the obtained samples were performed to investigate their structures, having a Bragg–Brentano diffractometer (D8_tools) in θ–2θ configuration with a Cu Kα line at 0.15418 nm as a source, while the transmission electron microscopy (TEM), high-resolution transmission electron microscopy (HRTEM), energy dispersive X-ray (EDX) (JEOL JEM-2100F operated at 200 kV), infrared spectroscopy (a Vertex 70 Fourier transform infrared (FTIR) spectrometer (Bruker)), and XPS (ESCALAB-250 performed with a monochromatic Al Kα (1486.6 eV) radiation source and a hemisphere detector with an energy resolution of 0.1 eV) experiments are carried out to characterize the morphology, microstructure and chemical bonding for the obtained samples. A UV–vis spectrophotometer (UV 2550, Shimadzu, Japan), in which $BaSO_4$ was used as a reflectance standard, and a LS-55 luminescence spectrometer were used to measure the optical properties for the samples. The leached Cd concentration in the supernatant was determined by a WFX-120 atomic absorption spectroscopy (AAS, Rayleigh Analytical Instrument Corp., China). Total organic carbon (TOC) was monitored using a Shimadzu TOC-500 Total Organic Carbon analysis system.

2.5. Measurements of photocatalytic degradation of MB

To examine the photocatalytic activity, the photodegradation of MB, which is a typical dye resistant to biodegradation, was investigated. A 300 W Xe lamp (PLS-SXE300, Beijing Trusttech Co., Ltd., China) as the light source, 80 milligrams photocatalyst of the pure CdS or the RGOC*x* (*x* = 1.0, 3.0, 5.0, 8.0, 12) was suspended, in an aqueous solution (500 mL) of 100 mg L^{-1} MB. Prior to the irradiation, the suspensions were magnetically stirred in the dark overnight to reach the absorption–desorption equilibrium of the dye on the surface of the photocatalyst. Then, the suspensions were placed in a reaction vessel equipped with a quartz window (exposed to light under dry-air flow to ensure a constant supply of oxygen), and the photocatalytic reactions lasted for 3 h. Aliquots (5 mL) were sampled and filtered through a cellulose filter (0.25 μm) to remove the suspended catalysts. The UV–visible absorption spectrum of the filtered solution was measured using a spectrophotometer (Optizen POP, Mecasys Co., Ltd., Seoul, South Korea) and the dye concentration was estimated by recording variations of the maximum absorption band (at 580 nm). The degradation efficiency *R* (%) can be calculated as:

$$R = \frac{C_0 - C}{C_0} \times 100\%$$

where C_0 is the initial concentration of dye and *C* is the revised concentration considering dye adsorption on the catalyst after photo-irradiation.

3. Results and discussion

3.1. Structure and morphology of the RGO/CdS

Fig. 2 shows the XRD patterns of pristine graphite, GO, and RGOC5.0, in which a very strong (0 0 2) peak in the XRD pattern of pristine graphite appears at $2\theta = 26.5°$, indicating a typical pattern of crystal graphitic structure with a layer–layer distance (*d*-spacing) of 0.334 nm (Fig. 2(a)), while for the GO a characteristic peak at $2\theta = 11.8°$ appears, corresponding to the interlayer spacing of $d_{002} = 0.848$ nm, which results from the presence of oxygen-containing functional groups formed during oxidation (Fig. 2(b)). The functional groups induce the GO to stack more loosely [43]. After the CdS nanoparticles spread on the RGO surface, significant changes are observed in the XRD pattern (Fig. 2(c)), from which the diffraction peaks appear at 2θ 26.5°, 43.8° and 52.1°, corresponding to the crystal plane (1 1 1), (2 2 0) and (3 1 1) for sphalerite CdS, respectively. The broad diffraction peaks in the

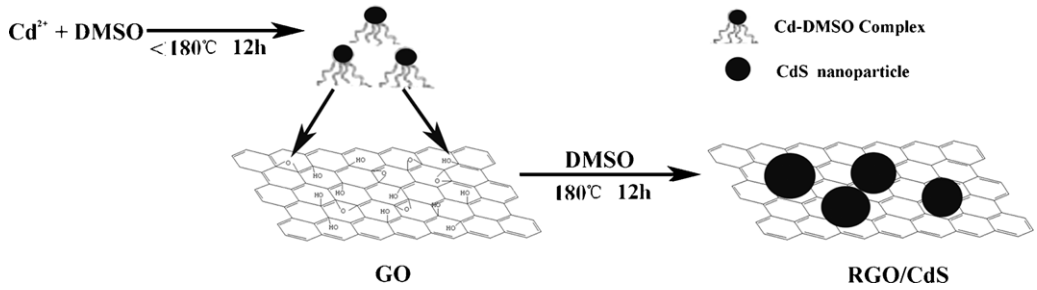

Fig. 1. Scheme of the one-step synthesis of RGO/CdS hybrid material.

XRD patterns indicate the grain size of CdS may be small. Based on Scherrer equation, the roughly estimated average grain size of CdS is about 6 nm on the RGO surface. It is well known that the attached nanoparticles may prevent the restacking of graphitic carbon sheets, and hence the characteristic diffraction peak of the layered structure will disappear. Nevertheless, even if the layered structure still exists, since the reduction of GO cannot be realized completely, the peak for GO(0 0 2) cannot appear at $2\theta = 26.5^\circ$. Therefore, the peak at $2\theta = 26.5^\circ$ for RGO/CdS is ascribed to CdS(1 1 1), rather than graphite or GO(0 0 2).

In order to reveal the microstructure for GO and RGO/CdS, TEM and HRTEM measurements are performed. Fig. 3 exhibits the TEM image for the GO, in which GO appears as a piece of waved silk veils. These GO sheets are transparent and entangled with each other. Fig. 4 shows the TEM images for RGO/CdS composites with different

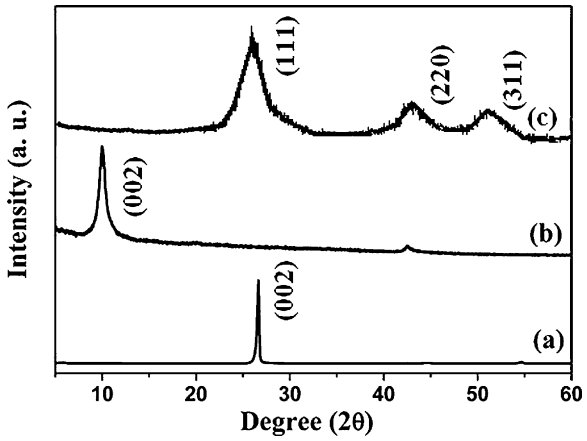

Fig. 2. X-ray diffraction patterns for the natural graphite powder (a), GO (b), and RGOC5.0 (c).

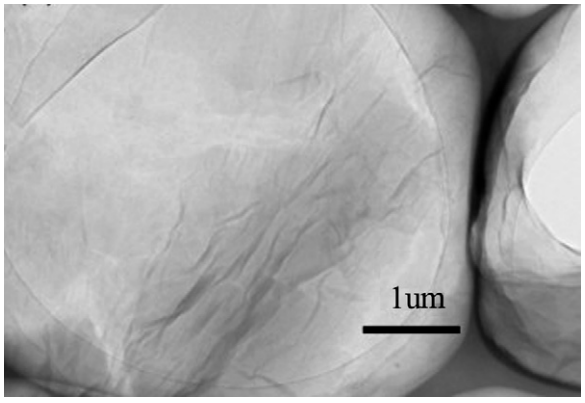

Fig. 3. TEM image of GO.

RGO contents (1.0 wt.%, 3.0 wt.%, 5.0 wt.%, 8.0 wt.% and 12.0 wt.%). In Fig. 4(a) and (b), the CdS nanoparticles are densely decorated on the RGO, whereas in Fig. 4(c)–(e), the CdS nanoparticles are sparsely dispersed on the RGO. Fig. 4(c) shows a well homogeneous distribution of CdS nanoparticles on the RGO surface. The inset of HRTEM image of the area A in Fig. 4(c) shows that there are a few nanocrystal particles ($d = 0.33$ nm), corresponding to the (1 1 1) plane of CdS. The density of CdS attached on the RGO surface decreases as the concentration of cadmium acetate decreases with increasing RGO contents, while the average particle–particle's distance (AP–PD) of CdS gradually increases. Fig. 4(f) shows the histogram for the AP–PD vs. catalysts, and give a direct evidence for the correlation between the nominal cadmium acetate content and the incorporated surface density of CdS nanoparticles. All above results clearly indicate that the denseness and crystallinity of CdS nanoparticles decorated on RGO can be altered by controlling the reaction parameters, meaning that the solvothermal method is very effective to prepare and deposit nanoparticles on the surface of RGO.

To better identify the elemental composition of the synthesized material, EDX measurements were carried out by the EDX spectrometer attached to TEM. One typical EDX spectroscopy for sample RGOC5.0, which is shown in Fig. 5, confirms the existence of Cd, S, C, and O elements (Cu peaks from the TEM grid). It is obvious that the C signal is attributed to the supporting RGO. The peak of O is observed, probably originating from the residual oxygenated groups of RGO, while Cd and S are from CdS particles. EDX quantitative microanalysis indicates that RGOC5.0 has a composition of Cd (31.5 at.%), S (29.2 at.%), C (37.4 at.%), O (1.9 at.%). The result determines the composition of CdS nanoparticles has attached on RGO.

3.2. Chemical bonding of RGO/CdS

X-ray photoelectron spectroscopy (XPS) is used to characterize the chemical bonding state of the atoms in GO and RGO/CdS, and the obtained data are calibrated by using the graphitic carbon at a binding energy of 284.6 eV. The deconvoluted C1s XPS spectrum of GO (Fig. 6(a)) shows four peaks at 284.6 eV (C—C, sp^2 bonded carbon), 285.6 eV (C—OH, hydroxyls), 286.7 eV (C—O, carbonyls) and 288.4 eV (O—C=O, carboxyl), indicating the high percentage of oxygen-containing functional groups [44,45]. Compared to GO, the peaks representing C—O and O—C=O for RGO/CdS almost vanish, while the intensity of the C—OH peak (Fig. 6(b)) decreases dramatically. This suggests that most of the oxygen-containing functional groups have been removed after reduction by DMSO. In addition, the hydroxyl (hydrophilic groups) remains on the RGO in RGO/CdS can enhance the dispersion of the hybrid material in the aqueous solution to a certain extent. It is worth noting that the degree of reduction of GO can be quantified by calculating the relative C/O ratio in the sample. From XPS spectra, the C/O ratio in GO (graphitic carbon, 53%) and RGO/CdS (graphitic carbon, 74%), can be estimated

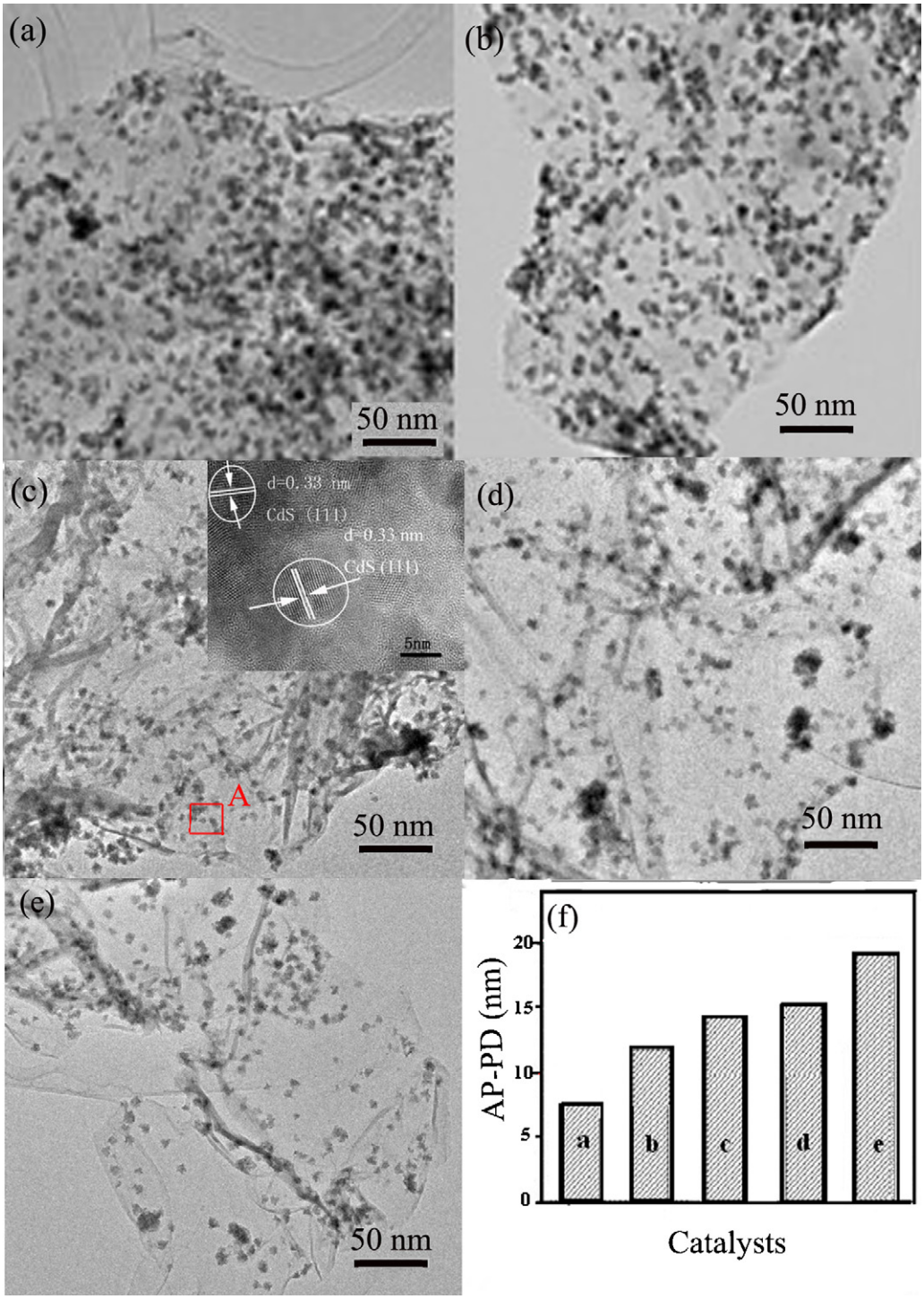

Fig. 4. TEM images for RGO/CdS hybrid nanostructures with different contents of RGO: RGOC1.0 (a), RGOC3.0 (b), RGOC5.0 (c), RGOC8.0 (d), RGOC12.0 (e). The histograms for AP–PD vs. catalysts (the AP–PD of each catalyst is obtained by computing the average of particle–particle's center distance of 200 nanoparticle pairs selected randomly) (f).

as 1.1:1 and 2.5:1, respectively, clearly demonstrating that the oxygenated groups in the GO have been substantially reduced during the synthesis process of RGO/CdS. Hence, the chemical reduction of GO was achieved by a simple solvothermal treatment effectively.

Further evidence comes from FTIR spectra. In Fig. 7(a), the representative FTIR peaks of the oxygen-containing functional groups of GO are observed at 1057 cm^{-1}, 1220 cm^{-1}, 1402 cm^{-1}, and 1724 cm^{-1} corresponding to alkoxy C—O stretching, phenolic C—OH stretching, carboxyl O—H stretching and C=O stretching of COOH groups situated at edges of the GO, respectively [46]. Furthermore, the broad band at 1624 cm^{-1} can be assigned to H—O—H bending band of the adsorbed H_2O molecules [47]. Compared with the peaks of the functional groups of GO, RGO/CdS shows a new absorption band (skeletal vibration of the GNs) at 1570 cm^{-1} [48], and much lower absorption intensity (Fig. 7(b)), which indicates the partial reduction of GO and is in good agreement with the XPS results.

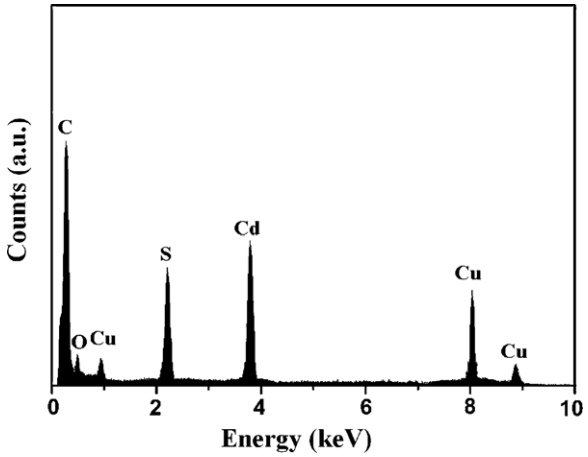

Fig. 5. EDX spectrum for RGOC5.0.

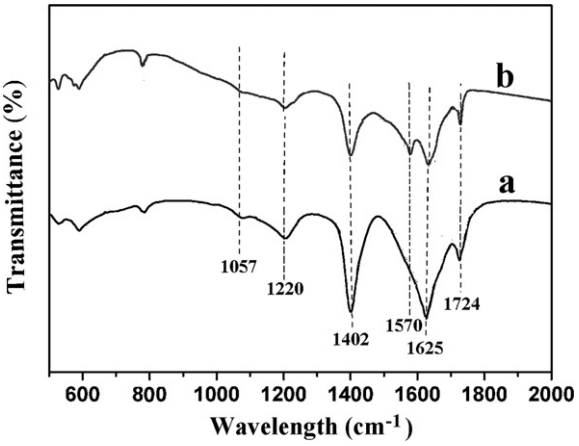

Fig. 7. FTIR spectra for GO (a) and RGOC5.0 (b).

3.3. Optical properties of RGO/CdS

Fig. 8(a) shows the UV–vis DRS for CdS (curve a), RGOC*x* (*x* = 1.0, 3.0, 5.0, 8.0, 12.0) (curves b–f) and RGO (curve g), wherein the absorbance intensity for RGO is significantly higher than other samples. Also, RGO/CdS samples have an enhanced absorbance intensity in the VL region (>530 nm) with increasing RGO contents (curves b–f), compared to CdS (curve a). This can be attributed to that the presence of carbon in the RGO/CdS reduces the reflection of light [49,50]. In addition, compared to CdS, there is an absorption edge for RGO/CdS, showing a gradual red shift, which suggests that the RGO could overlap part of the surface for CdS and absorb the visible light. Therefore, we believe that the introduction of RGO to CdS is more effective for the VL response, compared to CdS.

In order to study the effect of RGO on the recombination of e^-/h^+ pairs produced by CdS, the PL experiments for CdS, RGO and RGO/CdS are carried out, and the results are shown in Fig. 8(b). CdS shows a broad PL emission band at 620 nm (curve a). As expected, no specific PL response is observed in the range of 575–750 nm for RGO (curve g). After CdS nanoparticles spread on the RGO surface, a significant change is observed in the PL spectra, in which the PL intensity for RGO/CdS decreases gradually with increasing RGO content, indicating an efficient electron transfer from CdS nanoparticles to the RGO occurs. This leads to suppressing a charge recombination in RGO/CdS, compared to CdS (curves b–f). These results demonstrate that the RGO/CdS can effectively improve the optoelectronic property of CdS due to the introduction of RGO.

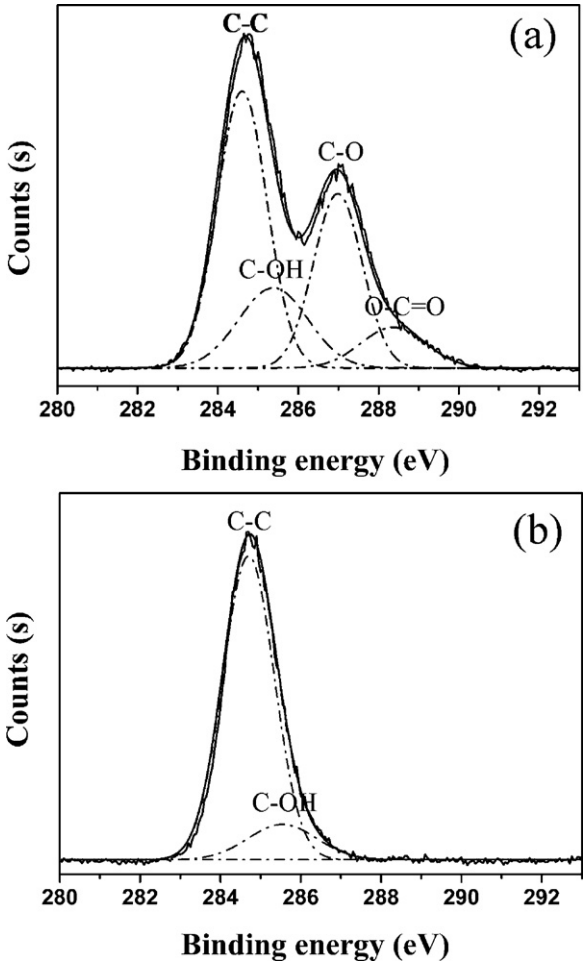

Fig. 6. XPS C1s spectra for GO (a) and RGOC5.0 (b).

3.4. Photodegradation of MB and the stability for RGO/CdS

Fig. 9(a) shows the profile of the photocatalytic degradation efficiency of MB for RGO, CdS and RGO/CdS under visible-light irradiation (λ > 420 nm). It can be seen that there is no any change for the concentration of MB for 3 h in the absence of catalysts. However, MB was slightly degraded in the presence of RGO due to its adsorption ability, which suggests that the degradation of MB results from the photocatalyst under light irradiation. The pure CdS exhibits a relatively low photodegradation efficiency (38%). The reason why CdS has a low degradation yield can be a result of the rapid recombination of conduction band (CB) electrons and valence band (VB) holes for CdS. However, there is a obvious much better photocatalytic degradation efficiency if RGO/CdS is used (RGOC*x*, *x* = 1.0, 3.0, 5.0) as the photocatalyst, comparing to CdS after the 3 h photoreaction, implying that the introduction of RGO as a support can improve the ability of CdS to degrade the organic pollutant under VL irradiation. The RGOC5.0 shows the highest photoactivity among all samples, whose photocatalytic degradation efficiency arrives at 94 wt.% and about 2.5 times higher than that of. This can be attributed to two reasons: firstly, the photocatalytic degradation efficiency will depends upon the availability of the OH and O_2 radical species, as stated in Eq. (5). While the production of the OH radical is expected to increase monotonically with increasing the CdS content the production of the O_2 radical should present a maximum. This maximum results from the reduction of the undecorated region as the CdS content increases, reaching a critical amount. Secondly, the photocatalytic degradation efficiency will also depends

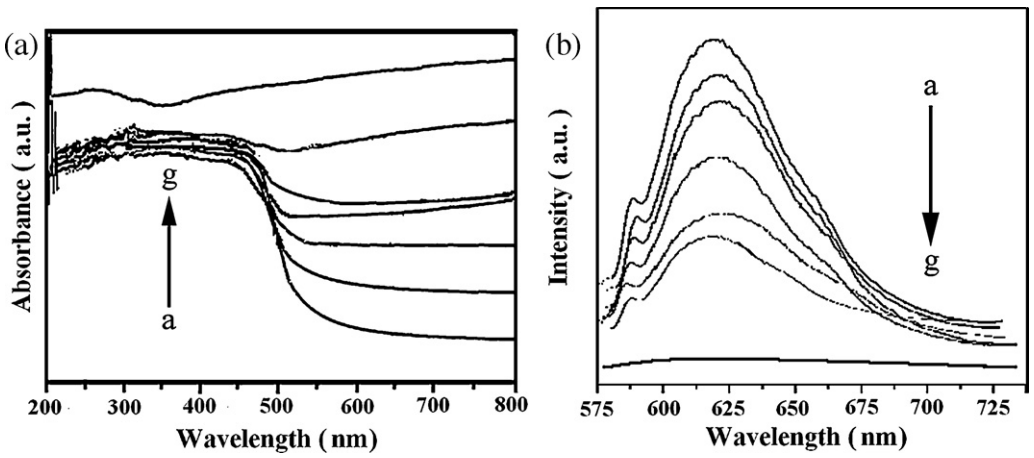

Fig. 8. UV–vis diffuse reflectance spectra (a) and PL spectra (b) for CdS (curve a), RGOC*x* (*x* = 1.0, 3.0, 5.0, 8.0, 12) (curve b–f), and RGO (curve g).

upon the efficiency at which the MB molecules approach the surface sites offering the required and concomitant OH and O_2 radical species. While the OH radical availability offered to MB is not hindered by the density of the CdS attached to the surface the O_2 radical availability offered to MB is expected to reduce as the density of the CdS attached to the surface reaches a critical value. That critical value (the density of the CdS attached to the surface) should be related to the average CdS particle–particle's distance that strictly hinders the close approach of the MB molecules to the O_2 radical species present at the undecorated surface region [51,52]. As a consequence, the RGOC5.0 with the optimum AP–PD presents the highest photocatalytic degradation efficiency. Upon further increasing RGO content (RGOC8.0 and RGOC12.0), the photocatalytic degradation efficiency for MB decreases, which can be attributed to the superfluous RGO in hybrid material will decrease the relative amount of CdS and increase light scattering, leading to shielding the active sites on the CdS nanoparticles surface and preventing CdS from absorbing the light. As a result, the photogenerated carriers passing through the reaction suspension solution is decreased, which has also been observed by other investigators [53,54].

The stability and reuse of the catalyst is crucial for its practical application. In order to avoid Cd ion leaching from catalyst to cause secondary pollution for water environment, the stability of the RGOC5.0 has been tested by monitoring the leached Cd content. The result shows no leaching of Cd ions from the RGOC5.0 as the photoreaction solution is detected during MB photodegradation at natural pH by AAS, indicating a high stability of RGO/CdS hybrid material. Otherwise, to monitor the stability of the RGOC5.0, we carry out experiments three times to test the recycle use of the photocatalysts by adding fresh MB solution (at the same initial concentration) after each run, and the results are shown in Fig. 9(b). The photocatalytic activity for RGOC5.0 reduces approximately 4% after the third run, and the photocatalytic degradation efficiency for RGOC5.0 after each 3 h run is 94%, 91% and 90%, respectively. This indicates that RGOC5.0 exhibits an excellent stability in the photocatalytic activity.

To further characterize photocatalytic ability of CdS and CdS/RGO hybrid material, TOC has been measured under VL irradiation and shown in Fig. 10. At 3 h, 57% of TOC is removed with the RGOC5.0 as MB is almost completely degraded. However, the removal of TOC is only 11% with CdS nanoparticles at this time. The TOC removal of CdS and RGOC5.0 reach 18% and 63%, respectively, by further increasing light irradiation time to 6 h. The result indicates that most of the organic intermediates are degraded and the mineralization of MB is largely completed. The TOC removal of CdS is less than that of the RGOC*x* (*x* = 1.0, 3.0, 5.0, 8.0, 12.0), which confirms that the introduction of RGO makes the CdS/RGO hybrid material exhibiting a higher mineralizing ability than CdS.

3.5. Mechanism for the enhancement of photocatalytic activity of CdS by RGO

Based on above results and discussion, we suggest a mechanism of the enhancement of photocatalytic activity of CdS by introduction of RGO under visible-light irradiation, as shown in Fig. 9. Under

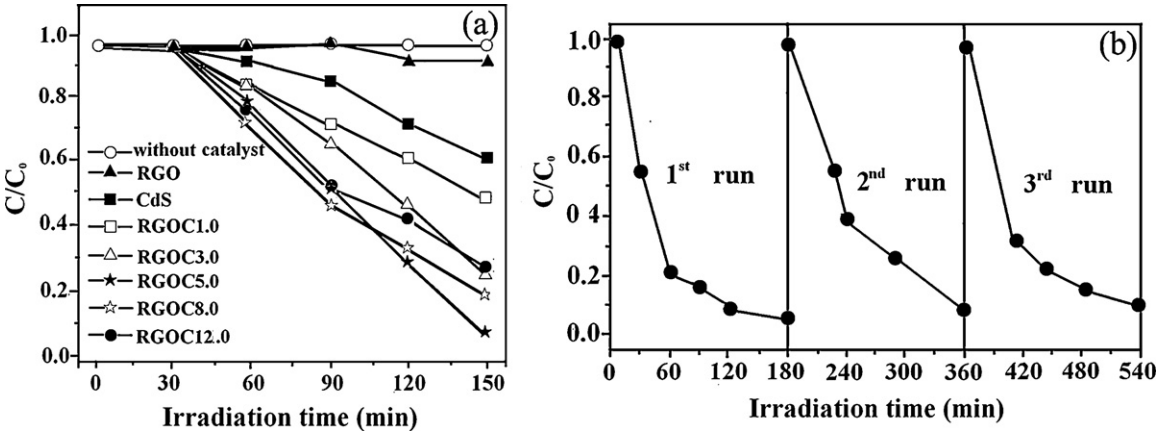

Fig. 9. Photo-degradation of MB without catalyst and with different photocatalysts for RGO, CdS, RGOC*x* (*x* = 1.0, 3.0, 5.0, 8.0, 12.0) (a) and Cycling runs in the photo-degradation of MB with RGOC5.0 (b).

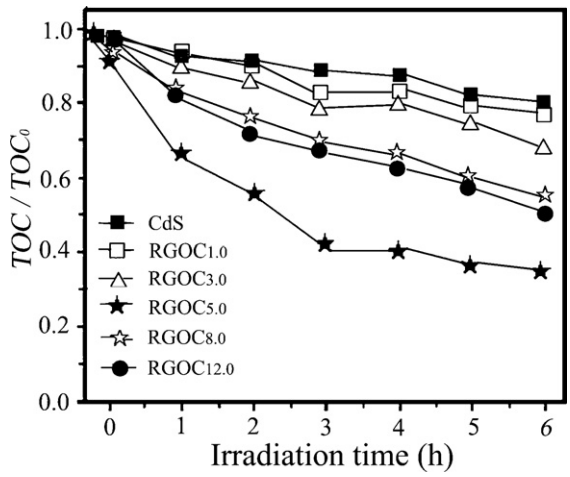

Fig. 10. The TOC removal of MB with CdS and RGOC*x* (*x* = 1.0, 3.0, 5.0, 8.0, 12.0).

irradiation by visible lamp, electrons (e^-) are excited from the VB to CB of the CdS semiconductor, leaving positive charged holes (h^+) in the VB (formula (1)). Without introduction of RGO, electrons will undergo a quick transition from CB to the VB owing to the instability of excited states, resulting in a low catalytic activity to the pollutant. Once RGO is introduced to the CdS nanoparticles, it can act as an electron acceptor and transporter to efficiently hinder the recombination the photogenerated electron–hole pairs. In the case of RGO/CdS, the electrons can be excited to CB in CdS, and meanwhile, the holes are produced in VB of CdS. The electrons of CB in CdS are easily transfer to carbon atoms in RGO, and these transferred electrons will have more opportunities to contact O_2, since O_2 molecules are adsorbed on the small portion of RGO undecorated CdS [1]. This leads to increasing the amount of oxygen peroxide radical $O_2^{\bullet-}$ (formula (2)). The optimum AP–PD can offer not only the available undecorated region to adsorb O_2 molecules effectively, but also the optimal approach accepting transferred electrons to O_2 forming $O_2^{\bullet-}$ [51,52]. In this work, an AP–PD of 14.8 nm for the RGOC5.0 exhibits the highest photoactivity for the MB molecules. On the other hand, the positive charged hole (h^+) may react with the OH^- derived from H_2O to form hydroxyl radical •OH, resulting in increasing the amount of hydroxyl radical •OH in RGO/CdS (formula (4) and (5)). The hydroxyl radical •OH has a high oxidative potential for the oxidation of organic pollutants. Thus, the MB molecule can be photocatalytically degraded by oxygen peroxide radical $O_2^{\bullet-}$ and hydroxyl radical •OH to CO_2, H_2O, and other mineralization [55,56], as shown in the following reaction formula (Fig. 11):

$$CdS + h\nu \rightarrow CdS \quad (h^+_{VB} + e^-_{CB}) \tag{1}$$

$$O_2 + e^-_{CB} \rightarrow O_2^{\bullet-} \tag{2}$$

$$H_2O \rightarrow H^+ + OH^- \tag{3}$$

$$OH^- + h^+_{VB} \rightarrow {}^{\bullet}OH \tag{4}$$

$$MB + {}^{\bullet}OH + O_2^{\bullet-} \rightarrow CO_2 + H_2O + \ldots \tag{5}$$

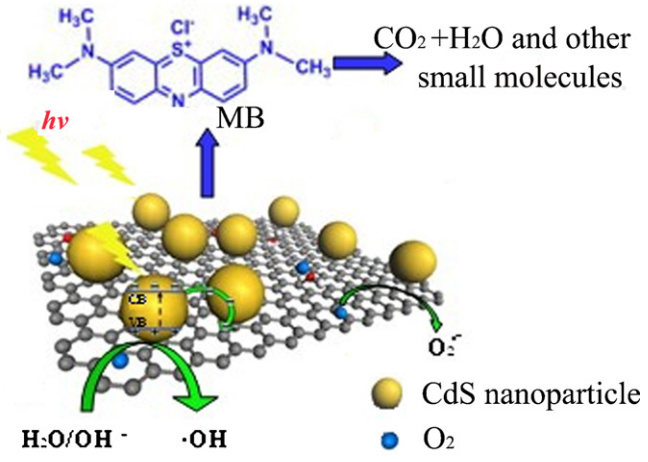

Fig. 11. Schematic illustration of the photo-degradation of MB molecules by RGO/CdS under VL irradiation.

4. Conclusions

A homogeneous distribution of CdS nanoparticles on RGO surface can be realized by using a facile solvothermal reaction. The RGO in RGO/CdS shows a photoluminescence quenching effect, leading to that the excited electrons under light irradiation transfer from the CdS nanoparticles to RGO so that the charge recombination in CdS can be effectively suppressed, compared to pure CdS. This effect is able to dramatically improve the photocatalytic activity of CdS nanoparticle for photo-degrading MB dye. The weight ratio of RGO to CdS in RGO/CdS has an evident effect on the photocatalytic activity of RGO/CdS if the mass of CdS is kept constant. The optimum weight percentage of RGO is found to be 5.0%, which exhibits the highest photocatalytic degradation efficiency (94%) and well stability for MB under VL irradiation. The increase in the photocatalytic degradation efficiency can be attributed to that RGO not only acts as a charge acceptor to promote the separation and transfer of photogenerated carriers, but also as a support to stabilize CdS and adsorb MB molecules in the aqueous solutions.

Acknowledgments

The support from National Natural Science Foundation of China (Grant Nos. 50525204, 50832001 and 51002061), the Fundamental Research Funds for the Jilin University (Grant No. 200903015), the special Ph.D. programme (Grant No. 200801830025) from MOE, the "211" and "985" project of Jilin University, China, the Science and Technology Development Programmer of Jilin Province (Grant No. 20090703), the Natural Science Foundation of Jilin Province (Grant No. 201115019), and the Program for Changjiang Scholars and Innovative Research Team in University are gratefully acknowledged.

References

[1] L.L. Ma, H.Z. Sun, Y.G. Zhang, L.L. Yu, J.L. Li, E.K. Wang, Y. Yu, M. Tan, J.B. Wang, Nanotechnology 19 (2008) 115709.
[2] R. Asahi, T. Morikawa, T. Ohwaki, K. Aoki, Y. Taga, Science 293 (2001) 269.
[3] Z. Zou, J. Ye, K. Sayama, H. Arakawa, Nature 414 (2001) 625.
[4] K. Maeda, K. Teramura, D. Lu, T. Takata, N. Saito, Y. Inoue, K. Domen, Nature 440 (2006) 295.
[5] R.M. Trommer, A.K. Alves, C.P. Bergmann, J. Alloys Compd. 491 (2010) 296–300.
[6] G. Liu, G.S. Li, X.Q. Qiu, L.P. Li, J. Alloys Compd. 481 (2009) 492–497.
[7] X.W. Zeng, Y.X. Gan, E. Clark, L.S. Su, J. Alloys Compd. 509 (2011) L221–L227.
[8] Y. Zhao, C.Z. Li, X.H. Liu, F. Gu, J. Alloys Compd. 440 (2007) 281–286.
[9] N.Z. Bao, L.M. Shen, T. Takata, K. Domen., Chem. Mater. 20 (2008) 110.
[10] H.J. Yan, J.H. Yang, G.J. Ma, G.P. Wu, X. Zong, Z.B. Lei, J.Y. Shi, C. Li, J. Catal. 266 (2009) 165.
[11] L.A. Silva, S.Y. Ryu, J. Choi, W. Choi, M.R. Hoffmann, J. Phys. Chem. C 112 (2008) 12069.
[12] Y.X. Li, G.F. Ma, S.Q. Peng, G.X. Lu, S.B. Li, Appl. Catal. A 363 (2009) 180.
[13] H. Fujiwara, H. Hosokawa, K. Murakosi, Y. Wada, S. Yanagida, J. Phys. Chem. B 101 (1997) 8270–8278.
[14] H. Yin, Y. Wada, T. Kitamura, S. Yanagina, Environ. Sci. Technol. 35 (2001) 227–231.
[15] B.A. Korgel, H.G. Monbouquette, J. Phys. Chem. B 101 (1997) 5010–5017.
[16] Q. Wang, G. Chen, C. Zhou, R.C. Jin, L. Wang, J. Alloys Compd. 503 (2010) 485–489.
[17] Y.Z. Fan, M.H. Deng, G.P. Chen, Q.X. Zhang, Y.H. Luo, D.M. Li, Q.B. Meng, J. Alloys Compd. 509 (2011) 1477–1481.

[18] W.X. Zhang, J.C. Cui, C.A. Tao, Y.G. Wu, Z.P. Li, L. Ma, Y.Q. Wen, G.T. Li., Angew. Chem. Int. Ed. 48 (2009) 5864.
[19] D. Li, M.B. Muller, S. Gilje, R.B. Kaner, G.G. Wallace, Nat. Nanotechnol. 3 (2008) 101.
[20] Y.X. Huang, X.W. Liu, J.F. Xie, G.P. Sheng, G.Y. Wang, Y.Y. Zhang, A.W. Xu, H.Q. Yu, Chem. Commun. 47 (2011) 5795.
[21] J.C. Liu, L. Liu, H.W. Bai, Y.J. Wang, D.D. Sun, Appl. Catal. B: Environ. 106 (2011) 76–82.
[22] H.L. Wang, H.S. Casalongue, Y.Y. Liang, H.J. Dai, J. Am. Chem. Soc. 132 (2010) 7472–7477.
[23] Y. Chen, X. Zhang, D.C. Zhang, Y.W. Ma, J. Alloys Compd. 511 (2012) 251–256.
[24] X.D. Huang, X.F. Zhou, K. Qian, D.Y. Zhao, Z.P. Liu, C.Z. Yu, J. Alloys Compd. 514 (2012) 76–80.
[25] J.C. Meyer, A.K. Geim, M.I. Katsnelson, K.S. Novoselov, T.J. Booth, S. Roth., Nature 446 (2007) 60.
[26] X.P. Shen, J.L. Wu, S. Bai, H. Zhou, J. Alloys Compd. 506 (2010) 136–140.
[27] T. Lv, L.K. Pan, X.J. Liu, T. Lu, G. Zhu, Z. Sun, J. Alloys Compd. 509 (2011) 10086–10091.
[28] G. Wang, T. Liu, Y.J. Luo, Y. Zhao, Z.Y. Ren, J.B. Bai, H. Wang, J. Alloys Compd. 509 (2011) L216–L220.
[29] B. Wang, Y. Wang, J.S. Park, H.J. Ahn, G.X. Wang, J. Alloys Compd. 509 (2011) 7778–7783.
[30] M. Feng, R. Sun, H. Zhan, Y. Chen, Nanotechnology 21 (2010) 07560.
[31] T.A. Pham, B.C. Choi, Y.T. Jeong, Nanotechnology 21 (2010) 465603.
[32] A. Cao, Z. Liu, S. Chu, M. Wu, Z. Ye, Z. Cai, Y. Chang, S. Wang, Q. Gong, Y. Liu, Adv. Mater. 22 (2010) 203.
[33] A. Lerf, H.Y. He, M. Forster, J.J. Klinowski., J. Phys. Chem. B 102 (1998) 4477.
[34] K.H. Ji, D.M. Jang, Y.J. Cho, Y. Myung, H.S. Kim, Y. Kim, J. Park, J. Phys. Chem. C 113 (2009) 19966–19972.
[35] Z.X. Cai, X.P. Yan, Nanotechnology 17 (2006) 4212–4216.
[36] Y.K. Kim, H. Park, Energy Environ. Sci. 4 (2011) 685–694.
[37] L. Jia, D.H. Wang, Y.X. Huang, A.W. Xu, H.Q. Yu, J. Phys. Chem. C 115 (2011) 11466–11473.
[38] Q. Li, B.D. Guo, J.G. Yu, J.R. Ran, B.H. Zhang, H.J. Yan, J.R. Gong, J. Am. Chem. Soc. 133 (2011) 10878–10884.
[39] T.Y. Peng, P. Zeng, D.N. Ke, X.Y. Liu, X.H. Zhang, Energy Fuels 25 (2011) 2203–2210.
[40] W.S. Hummers, R.E. Offeman, J. Am. Chem. Soc. 80 (1958), 1339–1339.
[41] H. Wang, L. Wang, C.Q. Qu, Y.D. Su, S.S. Yu, W.T. Zheng, Y.C. Liu, J. Solid State Chem. 184 (2011) 881–887.
[42] Q. Huang, L. Gao, Nanotechnology 15 (2004) 1855–1860.
[43] D.Y. Pan, S. Wang, B. Zhao, M.H. Wu, H.J. Zhang, Y. Wang, Z. Jiao, Chem. Mater. 21 (2009) 3136–3142.
[44] S. Stankovich, R.D. Piner, X.Q. Chen, N.Q. Wu, S.T. Nguyen, R.S. Ruoff, J. Mater. Chem. 16 (2006) 155.
[45] S. Stankovich, D.A. Dikin, R.D. Piner, K.A. Kohlhaas, A. Kleinhammes, Y.Y. Jia, Y. Wu, S.T. Nguyen, R.S. Ruoff, Carbon 45 (2007) 1558.
[46] T. Szabo, E. Tombacz, E. Illes, I. Dekany, Carbon 44 (2006) 537.
[47] Y.X. Xu, H. Bai, G.W. Lu, C. Li, G.Q. Shi, J. Am. Chem. Soc. 130 (2008) 5856.
[48] C. Nethravathi, M. Rajamathi, Carbon 46 (2008) 1994.
[49] X.Y. Zhang, H.P. Li, X.L. Cui, Y.H. Lin, J. Mater. Chem. 20 (2010) 2801.
[50] H.T. Yu, S. Chen, X.F. Fan, X. Quan, H.M. Zhao, X.Y. Li, Y.B. Zhang, Angew. Chem. Int. Ed. 49 (2010) 5106.
[51] Q.F. Yao, P.C. Morais., J. Appl. Phys. 93 (2003) 7385–7387.
[52] P.C. Morais, Q.F. Yao., J. Alloys Compd. 434–435 (2007) 565–568.
[53] Y. Yu, J.C. Yu, J.G. Yu, Y.C. Kwok, Y.K. Che, J.C. Zhao, L. Ding, W.K. Ge, P.K. Wong, Appl. Catal. A 289 (2005) 186–196.
[54] X.Y. Zhang, H.P. Li, X.L. Cui, Y.H. Lin, J. Mater. Chem. 20 (2010) 2801–2806.
[55] T.G. Xu, L.W. Zhang, H.Y. Cheng, Y.F. Zhu., Appl. Catal. B: Environ. 101 (2011) 382–387.
[56] H.Z. Chen, S.G. Yang, K. Yu, Y.M. Ju, C. Sun, J. Phys. Chem. A 115 (2011).